Supplementary Information

Deciphering the role of functional synergy in a catalytic molecular assembler: a *proof-of-concept* to boosted catalysis via retrosynthetic linker scissoring

Ranadip Goswami,[abc] Arun Karmakar, [ad‡] Sonal Rajput,[b‡] Manpreet Singh,[ab] Subrata Kundu *[ad] and Subhadip Neogi*[ab]

* Corresponding authors
[a] Academy of Scientific and Innovative Research (AcSIR), Ghaziabad- 201002, India
[b] Inorganic Materials & Catalysis Division, CSIR-Central Salt and Marine Chemicals Research Institute (CSIR-CSMCRI), Bhavnagar, Gujarat-364002, India
[c] Department of Applied Chemistry and Environmental Science, School of Science, RMIT University, Melbourne Victoria 3001, Australia
[d] Central Electrochemical Research Institute (CSIR-CECRI), Karaikudi, Tamil Nadu 630003, India
*E-mail:subrata_kundu2004@yahoo.co.in
*E-mail: sneogi@csmcri.res.in

[‡] Theses authors contributed equally.

1. Materials and methods

All the reagents employed were commercially available and used as provided without further purification. $Co(NO_3)_2 \cdot 6H_2O$, 2-amino terephthalic acid (2-ATA), 4-pyridinecarboxyaldehyde, and dithioxamide were purchased from S. D. Fine and TCI Chemicals, respectively. All of the solvents such as HPLC-grade *N*,*N*′-dimethylformamide (DMF), dichloromethane(DCM), acetone, ethanol, methanol, were procured from either Loba Chemie Pvt. Ltd., India or S. D. Fine Chemicals., India. All of the analytes used in this study were purchased from TCI Chemicals. NS Linker was prepared by following a literature method [1] and characterized by ESI-MS and NMR analysis. All spectroscopic, electrocatalytic and crystallographic studies are provided in the following sections.

2. Physical measurements

The infrared spectra (IR) of the samples were recorded using the KBr pellet method on a Perkin–Elmer GX FTIR spectrometer in the region of 400−4000 cm^{-1}. Powder X-ray diffraction (PXRD) data were collected using a PANalytical Empyrean (PIXcel 3D detector) system equipped with Cu Kα (λ=1.54 Å) radiation. Microanalyses of the compounds were conducted using elementarvario MICRO CUBE analyzer. Thermogravimetric analyses (TGA) (heating rate of 10 °C/min under N_2 atmosphere) were performed with a Mettler Toledo Star

SW 8.10 system. Prior to surface area measurement, sensing and electrocatalysis experiment, as-synthesized compounds were immersed in acetone for 3 days (exchanged with fresh acetone 3 times daily) at room temperature to replace lattice guest molecules. The solvent-exchanged frameworks were then degassed overnight under vacuum at 100 °C to generate **20a**. UV-Vis spectra recorded using Shimadzu UV-3101 PC spectrometer and the luminescence experiments were performed at room temperature using a Fluorolog Horiba JobinYvon spectrophotometer. Inductively coupled plasma-optical emission spectrometry (ICP-OES) analysis was measured by Perkin Elmer, Optima 2000. The XPS analysis was carried out using a Thermo Scientific ESCALAB 250 Xi photoelectron spectrometer (XPS) using a monochromatic Al K_α X-ray as an excitation source outfitted with an X-ray spot size of 650 × 650 μm^2.

3. Single Crystal X-ray crystallography

Single crystals with suitable dimensions were chosen under an optical microscope and mounted on a glass fibre for data collection. The crystal data for as synthesized brown-colored crystal of **CSMCRI-20** were collected on a Bruker D8 Quest diffractometer, with CMOS detector in shutter less mode. The crystals were cooled to low temperature using an Oxford Cryostream liquid nitrogen cryostat. The instrument was equipped with a graphite monochromatized MoKα X-ray source (λ = 0.71073 Å), with Triumph™ X-ray source optics. Data collection and initial indexing and cell refinement were handled using APEX II software.[1] Frame integration, including Lorentz-polarization corrections, and final cell parameter calculations were carried out using SAINT+ software.[2] The data were corrected for absorption using the SADABS program.[3] Decay of reflection intensity was monitored by analysis of redundant frames. The structure was solved using Direct methods and difference Fourier techniques. All non-hydrogen atoms were refined anisotropically. All H atoms were placed in calculated positions using idealized geometries (riding model) and assigned fixed isotropic displacement parameters. The SHELXL-2014 package within the OLEX2 crystallographic software [4-7] was applied for structure refinement with several full-matrix least-squares/difference Fourier cycles. The disordered guest solvent molecules in the crystal lattice were treated with solvent mask option in OLEX2 software.[4] The potential solvent accessible void space was calculated using the PLATON[8] software. The crystal and refinement data for solvent free **CSMCRI-20** is listed in Table S2. Topological analysis was performed by using TOPOSPro software.[9]

4. Experimental section

a) Synthetic protocol of NS linker

A mixture of 200 mg of dithiooxamide (1.66mmol) and 0.4ml of 4-pyridinecarboxaldehyde (4.4 mmol) in 20ml DMF were heated at 150 °C with constant stirring for 2.5 hours under N_2 atmosphere. The reaction mixture was cooled to room temperature and a yellow crystalline product were precipitated out, which was collected by filtration, washed with fresh H_2O until the colour of the filtrate turned out colourless and dried under air (311 mg, 63% yield). (Scheme 1).The ^{1}H NMR spectrum of the product was in good agreement with that of NS linker reported in literature. [10]

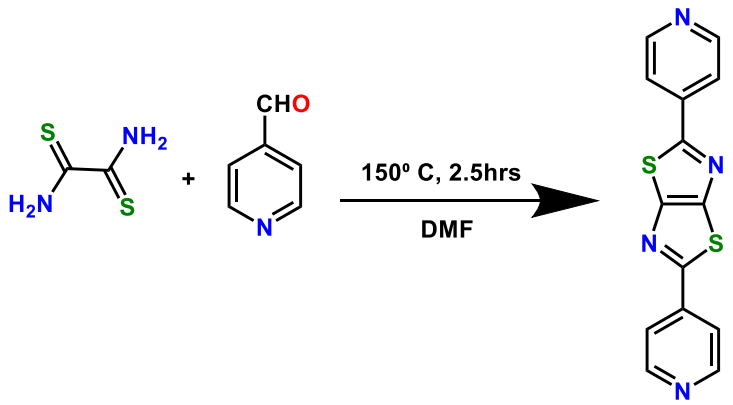

Scheme S1. Schematic synthetic protocol of NS Linker.

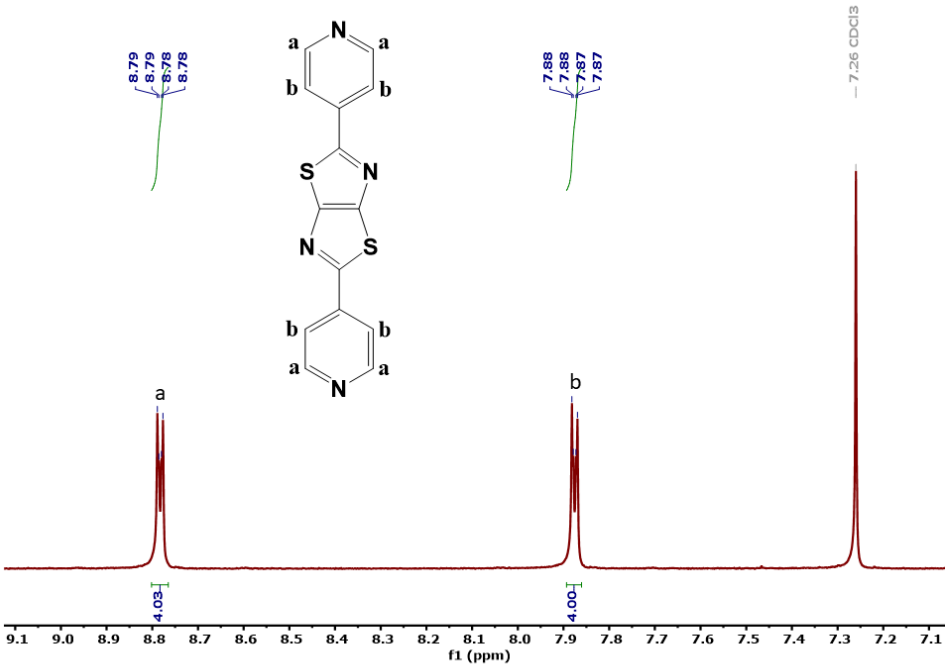

Fig. S1. ^{1}H NMR of NS linker.

(a)

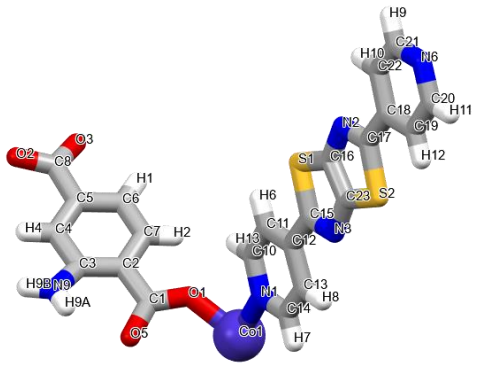

(b)

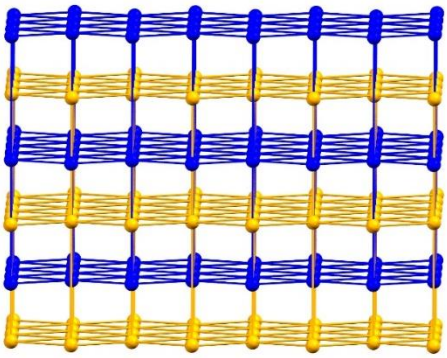

(c)

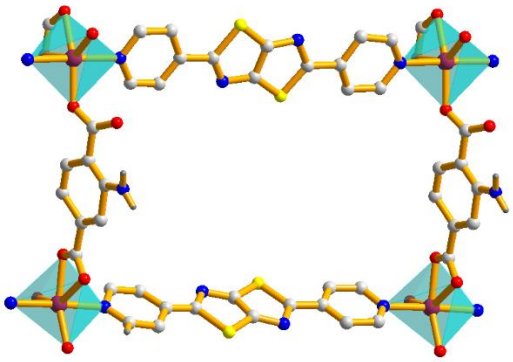

(d)

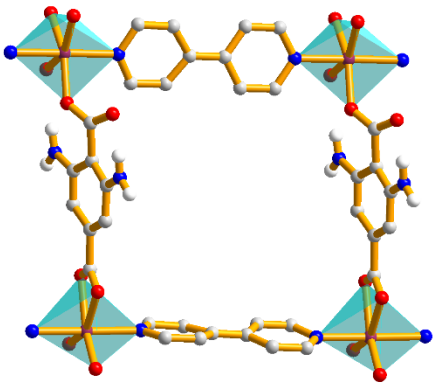

(e)

(f)

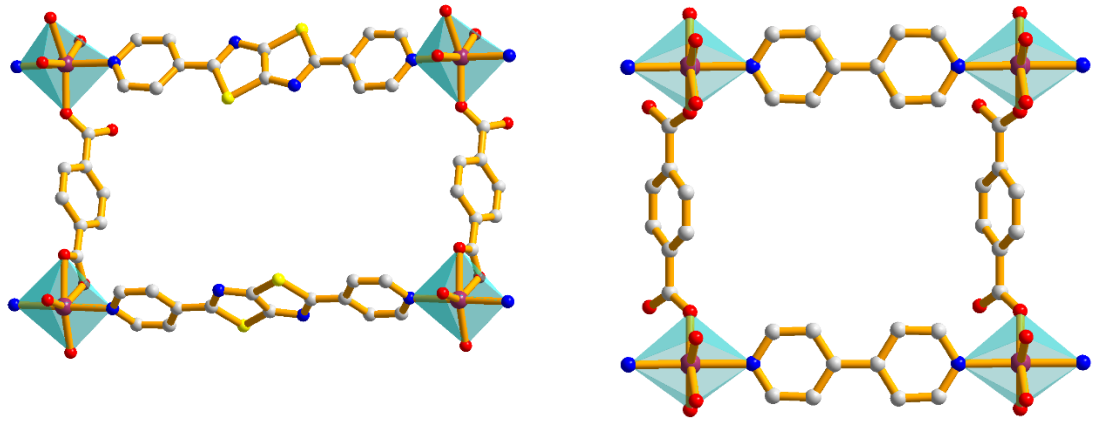

Fig. S2. (a) Asymmetric unit, and (b) Topological representation of **CSMCRI-20**. View of the four MOFs used in this study, including (c) **CSMCRI-20**, (d) 2-ATA-BPY (the –NH_2 groups are disordered over two positions), (e) BDC-NS, and (f) BDC-BPY.

(a)

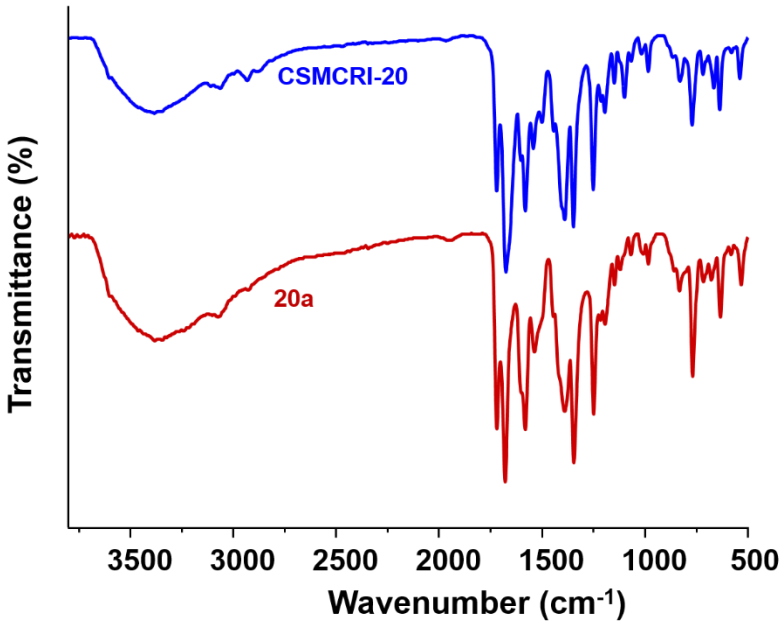

(b)

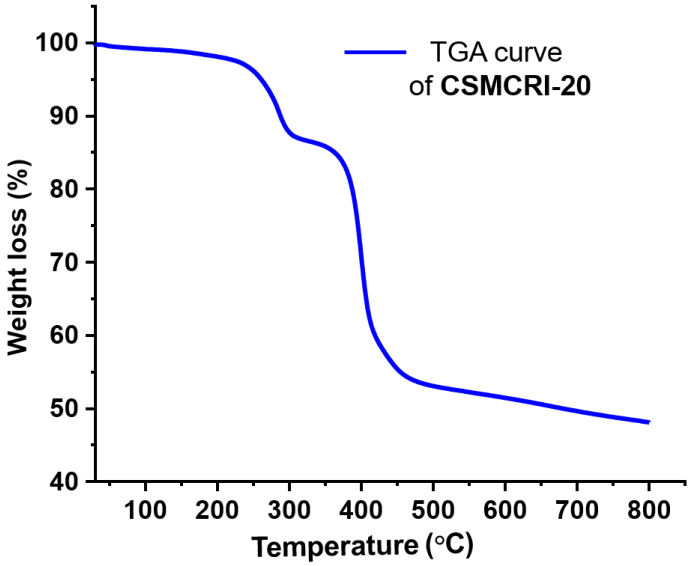

Fig. S3. (a) FT-IR profile of as-synthesized and activated framework. (b) Thermogravimetric analysis of as-synthesized **CSMCRI-20**.

(a)

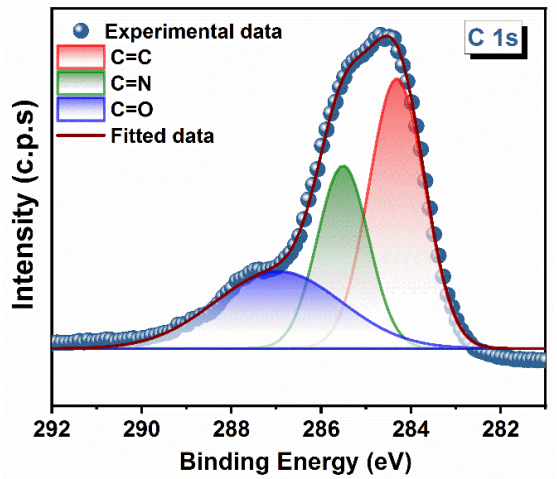

(b)

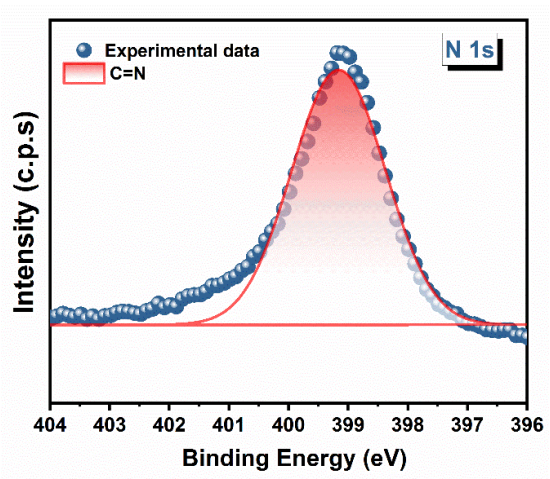

(c)

(d)

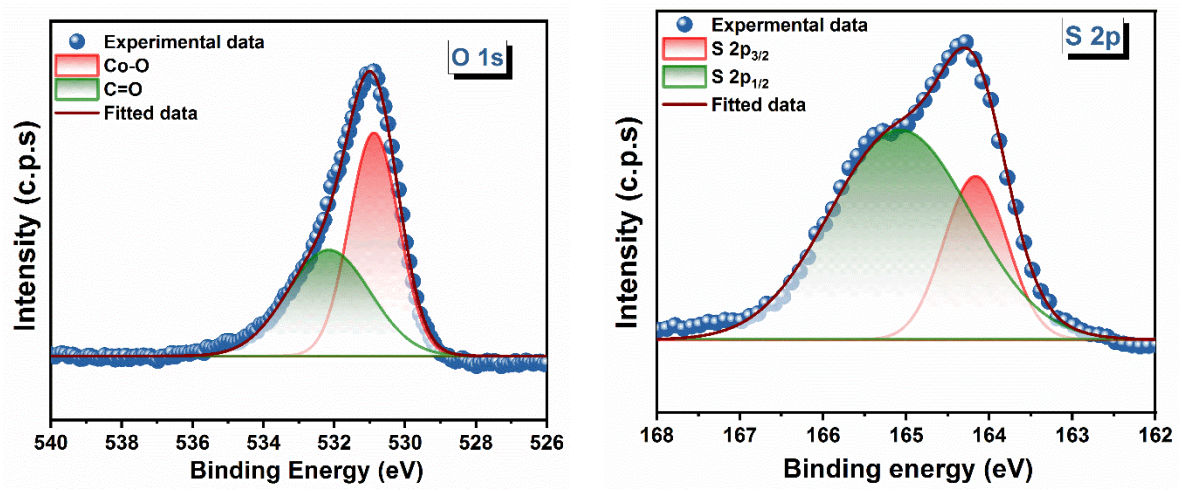

Fig. S4. XPS survey spectrum of **CSMCRI-20**. Deconvoluted spectrum of a) C 1s (b) N 1s (c) O 1s and (d) S 2p.

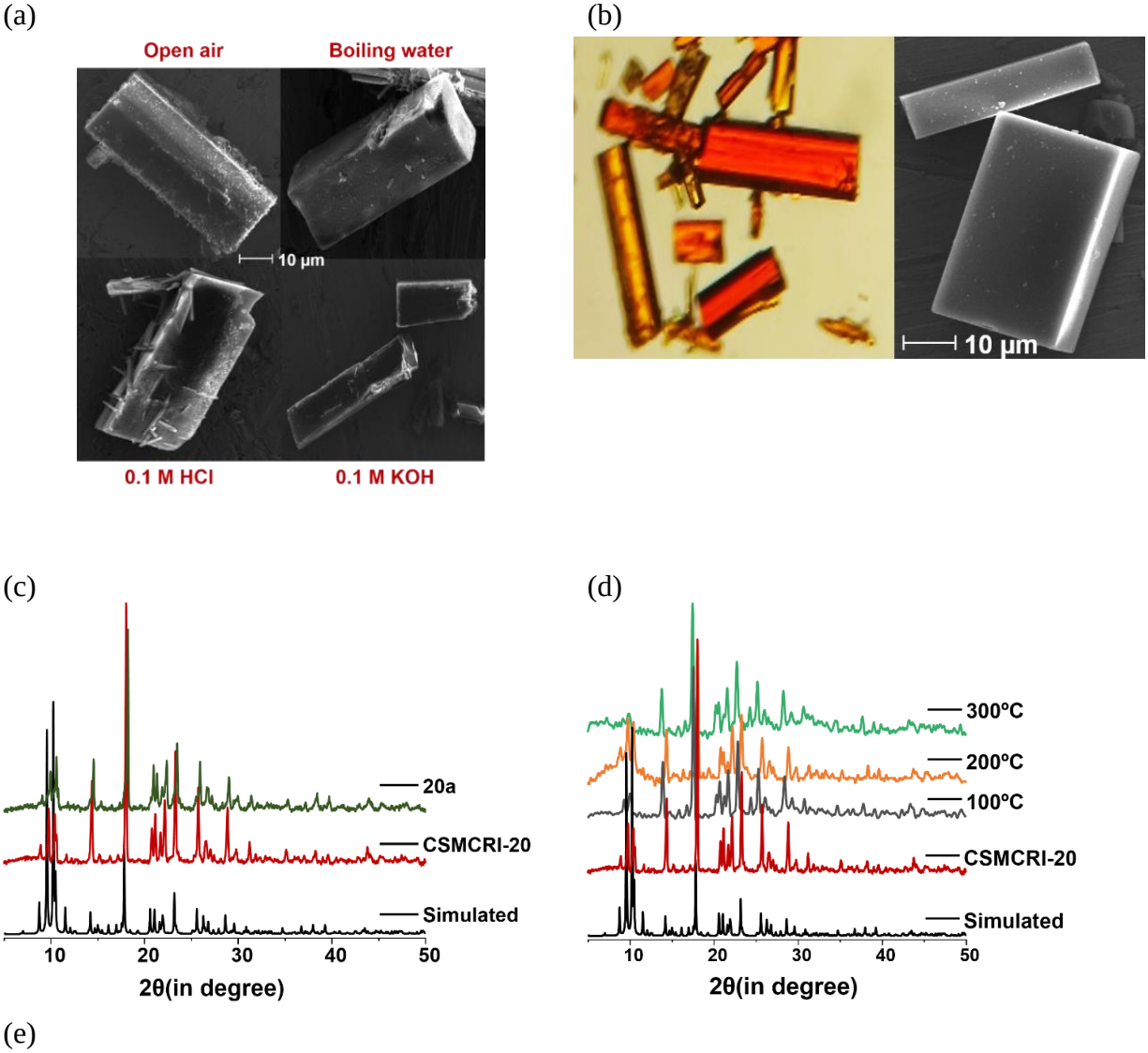

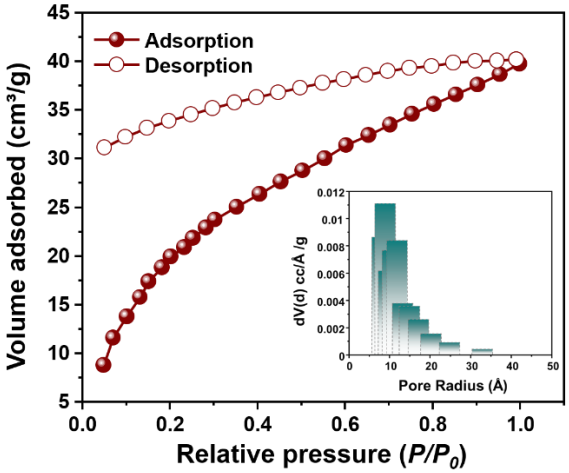

Fig. S5. (a) FE-SEM images after exposure of **CSMCRI-20** to harsh conditions (b) digital and FE-SEM images of **CSMCRI-20** c) Simulated, as synthesized and activated PXRD patterns of **CSMCRI-20**. (d) Variable temperature PXRD pattern of **CSMCRI-20**. (e) CO_2 sorption and pore size distribution of **20a** at 195 K.

3. a) Calculations of the electrochemical assessable surface area (EASA)

The Electrochemical Assessable Surface Area (EASA) of the MOF catalyst (**20a**) was calculated by measuring electrochemical double layer capacitance (C_{dl}) for the MOF and specific electrochemical double layer capacitance (C_s) of an atomically smooth surface by using the following equation:

EASA= C_{dl}/C_s

The electrochemical double layer capacitance i.e. C_{dl} for **20a** was obtained by measuring the CVs at various scan rates (150 mV/s to 30 mV/s) in the non-Faradaic region. The slope of the plot of capacitive current as a function of scan rate in the non-faradaic region is the value of C_{dl} for the MOF catalyst. In our study, specific electrochemical double layer capacitance of an atomically smooth surface (C_s) was taken as 0.040 mF cm^{-2}.

b) Calculation of Roughness Factor (R_f):

Roughness Factor for activated **CSMCRI-20** was calculated by the following equation,

Roughness factor (R_f) = EASA/ geometrical area of the working electrode

Here, the geometrical surface area of the working electrode was 0.5 cm^2.

c) Calculation of Faradaic efficiency (FE %):

The Faradaic efficiency (FE) information the catalyst is calculated by using the Faraday's second law of electrolysis as given below:

$$m = \frac{M \times I \times t}{N \times F} \quad \ldots\ldots\ldots\ldots\ldots\ldots\ldots\ldots\ldots\ldots (1)$$

m = faradaic efficiency; M = molecular weight of O_2; I = Current density at certain applied potential; t = time in hour; N = number of electron transfer (here N = 4) and F = Faraday constant = 96485 C/mol. Here amount of gas was measured by GC-MS and applied potential was 1.6 V vs RHE. The experimentally measured amount of gas with different time interval were measured and compared theoretical amount of O_2 that can be produced.

d) Calculation of Turn-over Frequency (TOF):

Serial number	Compound	No. of atoms per unit cell	Crystal volume ($Å^3$)
1	**CSMCRI-20**	8	5291
2	**BDC-NS**	8	10169.1
3	**2-ATA-BPY**	2	3538.14
4	**BDC-BPY**	4	1698.4

1. For **CSMCRI-20** number of per unit surface area = [(8 atom/unit cell) / (5291 $Å^3$/unit cell)]$^{2/3}$

   $= 1.5 \times 10^{20}$

2. For **BDC-NS** number of per unit surface area = [(8 atom/unit cell) / (10169.1 $Å^3$/unit cell)]$^{2/3}$

   $= 4.73 \times 10^{20}$

3. For **2-ATA-BPY** number of per unit surface area = [(2 atom/unit cell) / (3538.14 $Å^3$/unit cell)]$^{2/3}$

   $= 3.4 \times 10^{20}$

4. For **BDC-BPY** number of per unit surface area = [(4 atom/unit cell) / (1698.4 $Å^3$/unit cell)]$^{2/3}$

   $= 1.41 \times 10^{21}$

TOF = Number of O_2 turnover/ number of metal ions

The number of O_2 turnovers was calculated using the current density at 430 mV overpotential *via*:

Number of O_2 turnover per unit surface area

= **(**J mA/cm^2**) × (**1 {C/s}/1000 mA**) × (**1 {mol e$^-$}/96845 C**) × (**1 mol O_2/ 4 {mol e$^-$}**) × (**6.023 × 1023 mol O_2/ 1 mol O_2**)**

$= J \times 15.612 \times 10^{14}\ sec^{-1}\ mA\ cm^{-2}$

TOF $_{CSMCRI-20}$@430 mV overpotential $= [J \times 15.612 \times 10^{14}\ sec^{-1}\ mA\ cm^{-2}]/ [(1.5 \times 10^{20})]$

$= [38.8\ mA \times 15.612 \times 10^{14}\ sec^{-1}\ mA\ cm^{-2}] / [(1.5 \times 10^{20})]$

$= 1.355 \times 10^{-4}\ sec^{-1}$

TOF$_{BDC-NS}$@430 mV overpotential

$= [9.35\ mA \times 15.612 \times 10^{14}\ sec^{-1}\ mA\ cm^{-2}] / [(4.73 \times 10^{20})]$

$= 3.08 \times 10^{-5}\ sec^{-1}$

TOF$_{2-ATA-BPY}$@430 mV overpotential

$= [9.28\ mA \times 15.612 \times 10^{14}\ sec^{-1}\ mA\ cm^{-2}] / [(3.4 \times 10^{20})]$

$= 4.26 \times 10^{-5}\ sec^{-1}$

TOF$_{BDC-BPY}$@430 mV overpotential

$= [5.29\ mA \times 15.612 \times 10^{14}\ sec^{-1}\ mA\ cm^{-2}] / [(1.41 \times 10^{21})]$

$= 5.8 \times 10^{-6}\ sec^{-1}$

Sl. No	Compound	No of atom per cm^2	Current density@430 mV overpotential	TOF
1	**CSMCRI-20**	1.5×10^{20}	38.8 mA/cm^2	$4.03 \times 10^{-4}\ sec^{-1}$
2	**BDC-NS**	4.73×10^{20}	9.35 mA/cm^2	$3.08 \times 10^{-5}\ sec^{-1}$
3	**2-ATA-BPY**	3.4×10^{20}	9.28 mA/cm^2	$4.26 \times 10^{-5}\ sec^{-1}$
4	**BDC-BPY**	1.41×10^{21}	5.29 mA/cm^2	$5.8 \times 10^{-6}\ sec^{-1}$

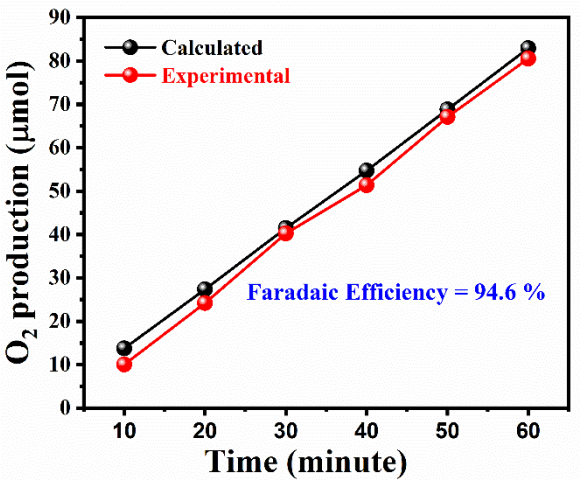

Fig. S6. Total accumulated charge during bulk electrolysis at certain interval of time.

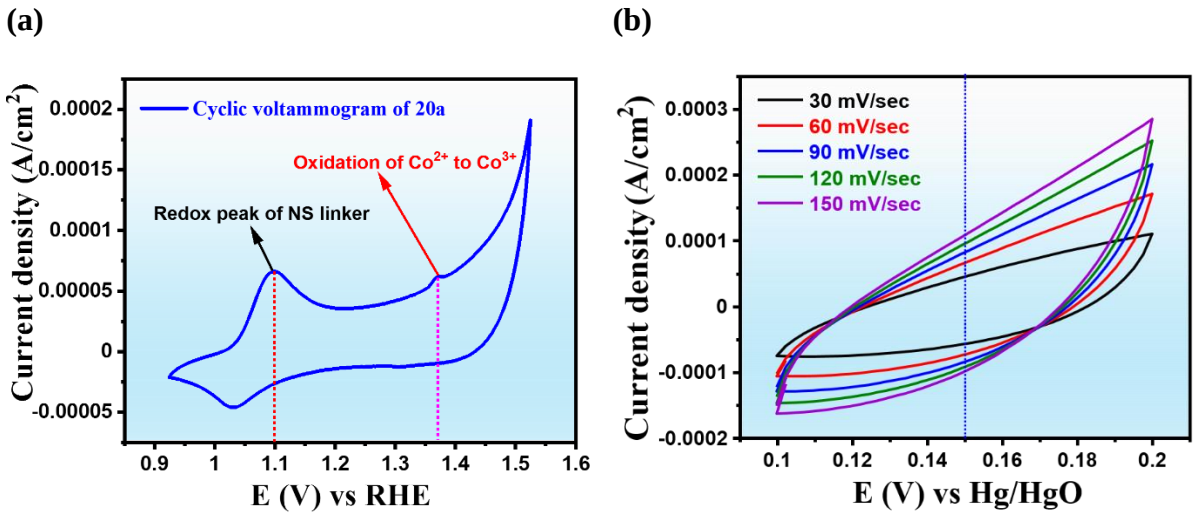

Fig. S7. (a) Cyclic voltammogram of **20a**. (b) Cyclic voltammetry plot for **20a** at various scan rates (150 mV/s to 30 mV/s) in the non-Faradaic region.

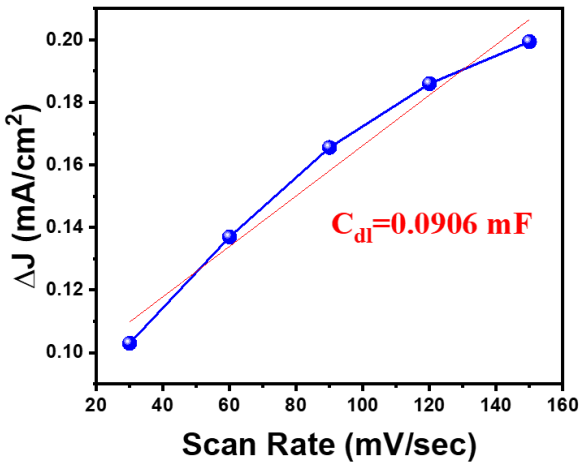

Fig. S8. Plot of capacitive current as a function of scan rate for **20a** in the non-Faradaic region.

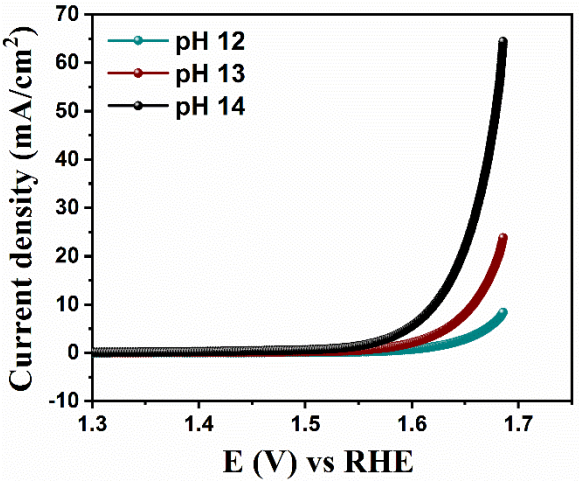

Fig. S9. LSV for **20a** in KOH solution with different pH values at fixed scan rate (5mV s^{-1}).

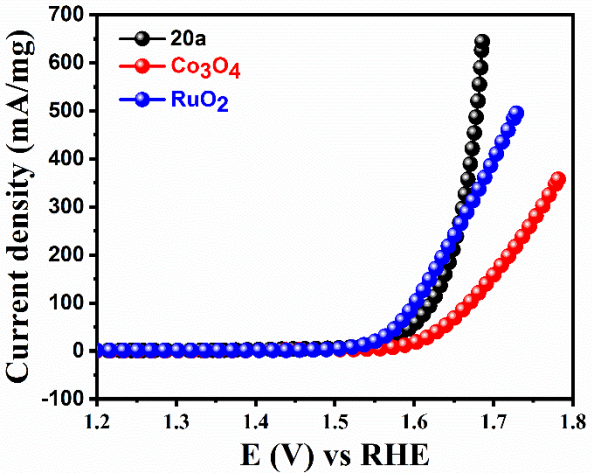

Fig. S10. Mass activity normalized LSV curve for **CSMCRI-20**.

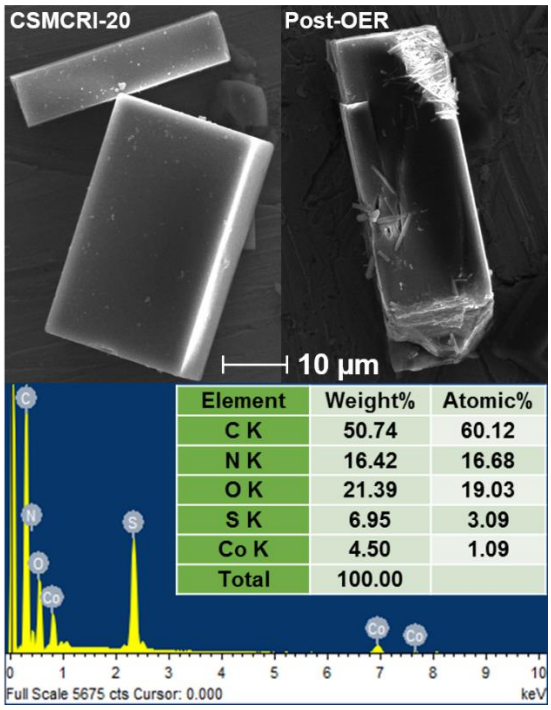

Fig. S11. FE-SEM images of **CSMCRI-20** and material after 1000 cycles of OER analysis, revealing that block-shaped morphology is well retained (*top*). SEM-EDX analysis (below) of the material after OER.

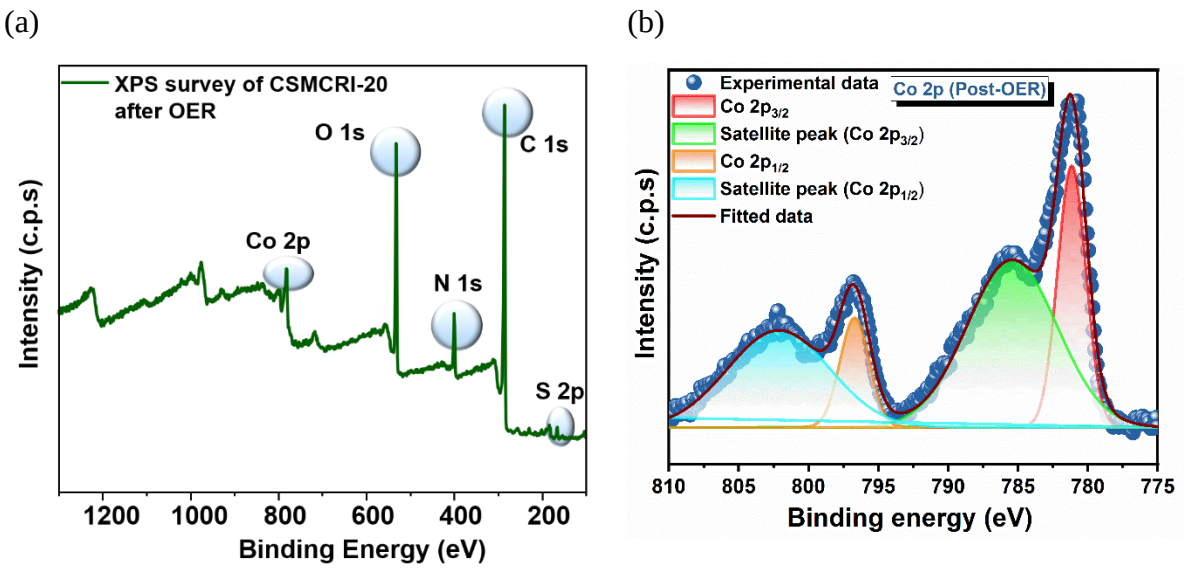

Fig. S12. a) XPS survey spectrum and b) deconvoluted Co 2p XPS spectrum after 500 cycles of OER analysis.

(a)

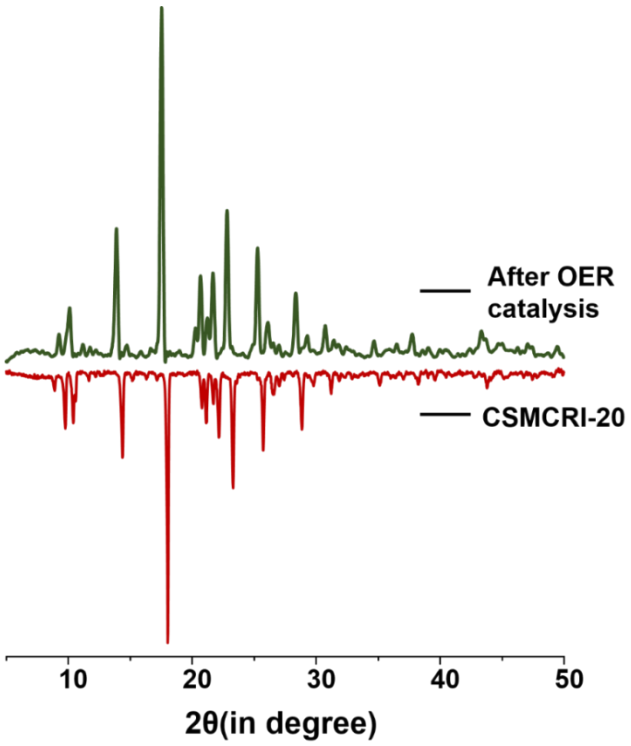

(b)

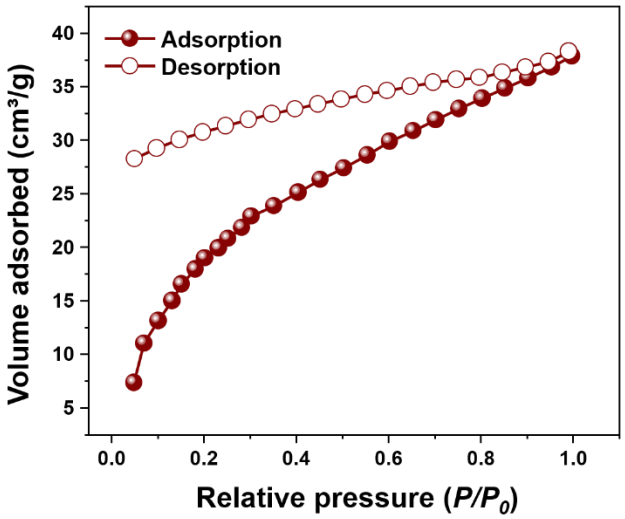

Fig. S13. (a) PXRD pattern of **20a**, obtained after 1000 cycles of OER analysis and (b) CO_2 sorption of **20a** after OER analysis in 1 M KOH at 195 K.

Table S1. Optimization of reaction conditions for the friedel-crafts alkylation between indole and *β*-nitrostyrene using **20a**.

Entry[a]	Catalyst	Catalyst Mol (%)	Time	Solvent	Temp (°C)	Conversion[b] (%)
1.	**20a**	9	9	Toluene	RT	15
2.	**20a**	8	12	Toluene	60	21
3.	**20a**	8	9	Acetonitrile	RT	30
4.	**20a**	9	12	Acetonitrile	60	46
5.	**20a**	9	9	DCM	RT	47.8
6.	**20a**	9	6	DCM	45	48.7
7.	**20a**	9	9	DCM	60	78.7
8.	**20a**	9	12	DCM	60	100
9.	**20a**	5	12	DCM	60	77.5
10.	**20a**	5	24	DCM	60	98
11.	**20a**	9	24	DCM	RT	51.5

[a]Entries 1-11 were performed using catalyst **20a**. [b]Conversion was determined by ^{1}H NMR spectroscopy.

4. a) Monitoring the progress of the reaction

Progress of the reaction was monitored by ^{1}H NMR spectroscopy through the integration of the α-vinyl and β-vinyl protons of β-nitrostyrene (δ 8.00−8.06 ppm) and the resulting aliphatic proton of the product 3-(2-nitro 1-phenylethyl)-^{1}H- indole (δ 4.92−5.25 ppm). So as to perform the catalyst recycling test, the used catalyst (separated by centrifugation) was washed with DCM and dried at 100 ^{0}C for 4 h under vacuum. Regenerated material was used further to perform the catalytic experiment and procedure was repeated for next 5 cycles.

b) Calculation of the % conversion

Total amount of complex = unreacted β-nitrostyrene + 3-(2-nitro-1-phenylethyl)-^{1}H-indole = 1.015 +2.12 = 3.135

Percentage of the unreacted β-nitrostyrene: (100/3.135) % = 31.89%

Conversion of β-nitrostyrene = (100-31.89) % = 68.1%.

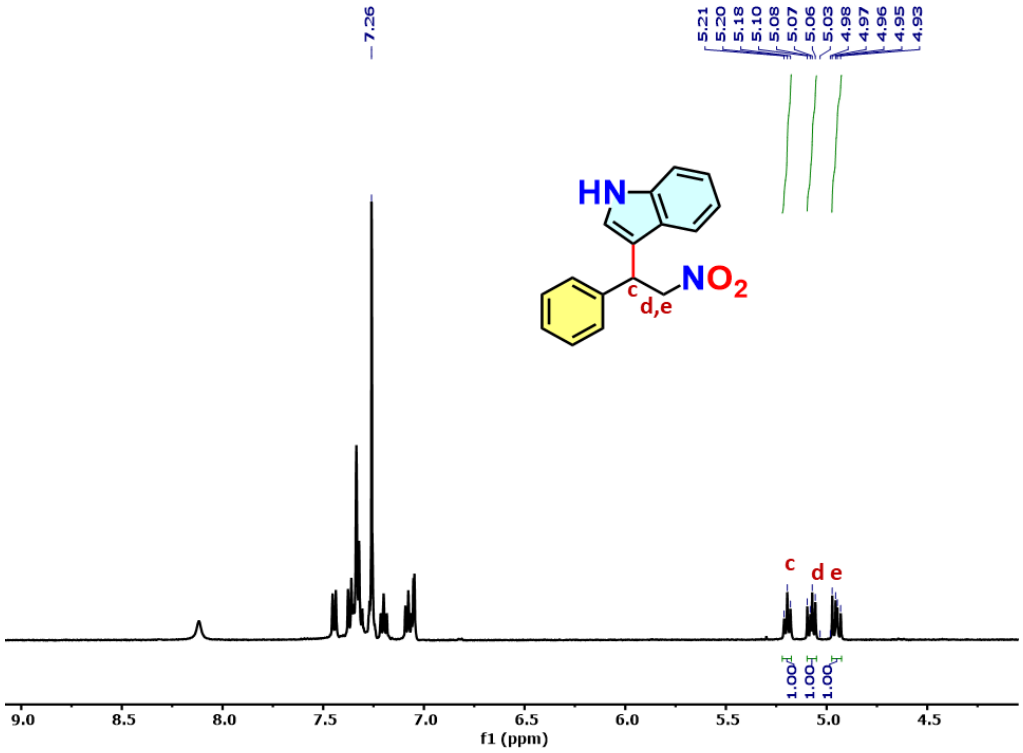

Fig. S14. Integration in the ^{1}H NMR spectrum for the determination of conversion (%) of the reaction product catalyzed by **20a** (Table 2, entry 1).

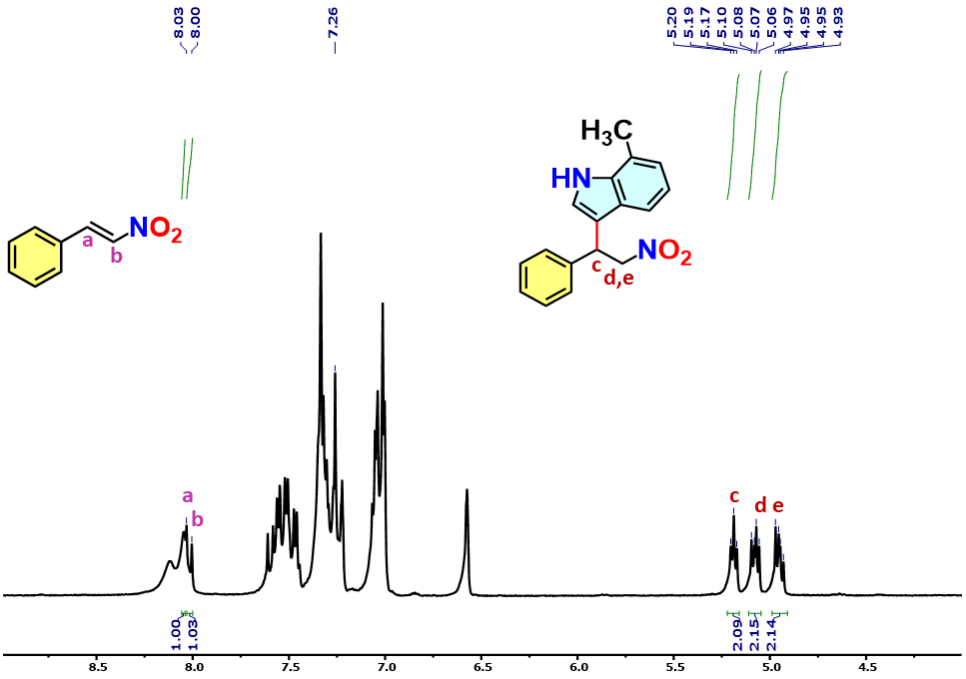

Fig. S15. Integration in the ^{1}H NMR spectrum for the determination of conversion (%) of the reaction product catalyzed by **20a** (**Table 2, entry 2**).

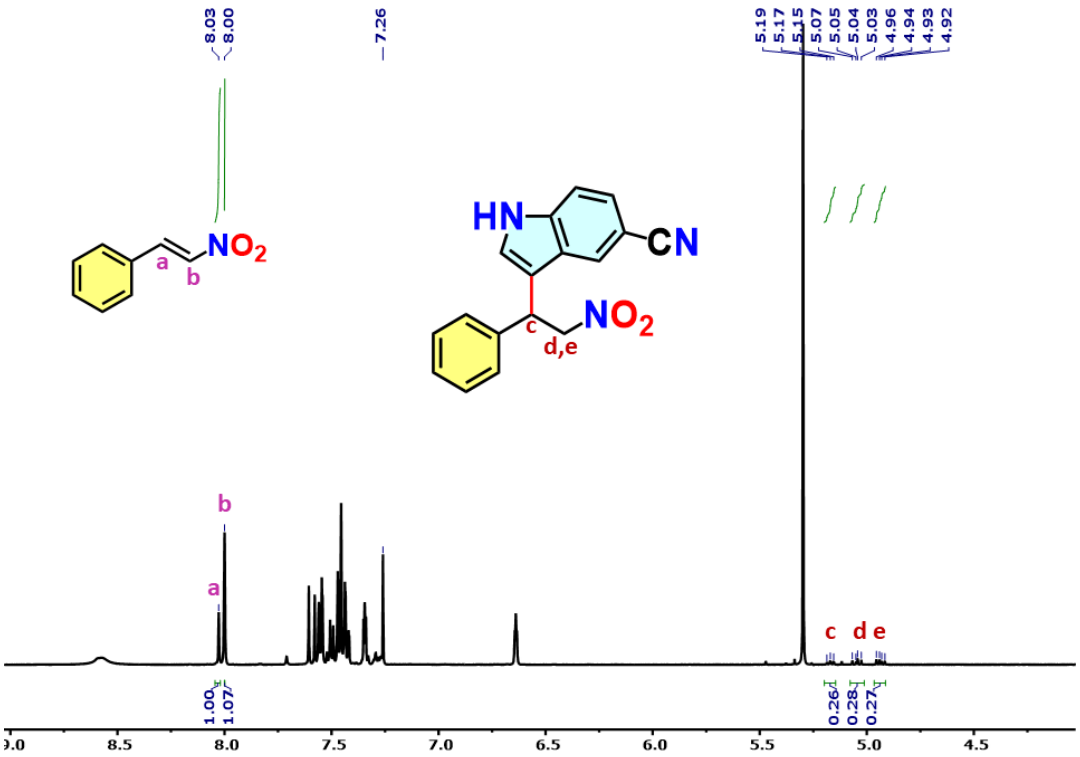

Fig. S16. Integration in the ^{1}H NMR spectrum for the determination of conversion (%) of the reaction product catalyzed by **20a** (**Table 2, entry 3**).

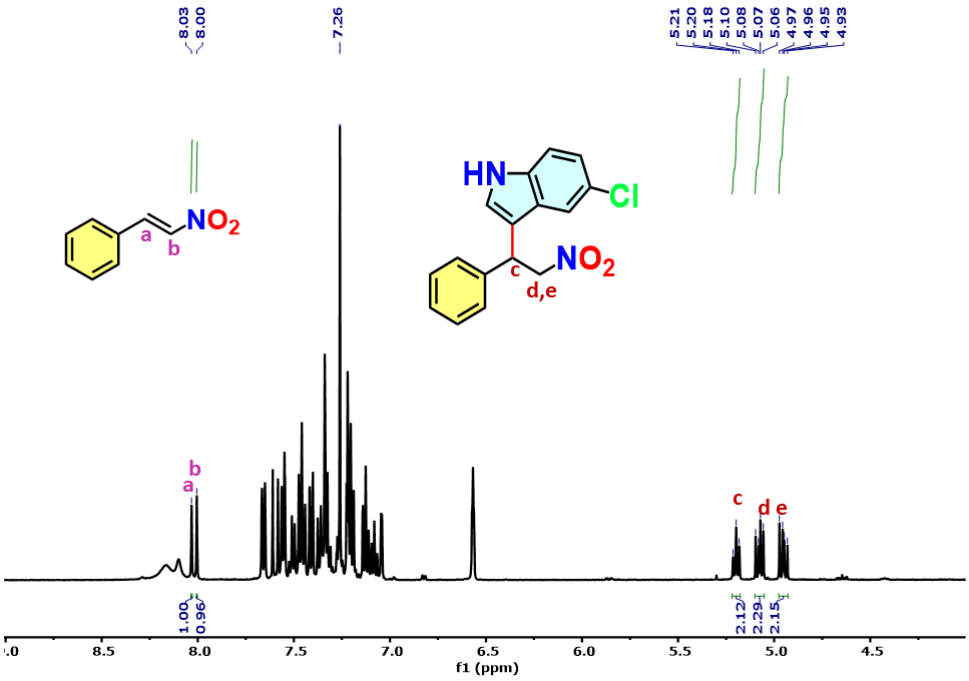

Fig. S17. Integration in the ^{1}H NMR spectrum for the determination of conversion (%) of the reaction product catalyzed by **20a (Table 2, entry 4).**

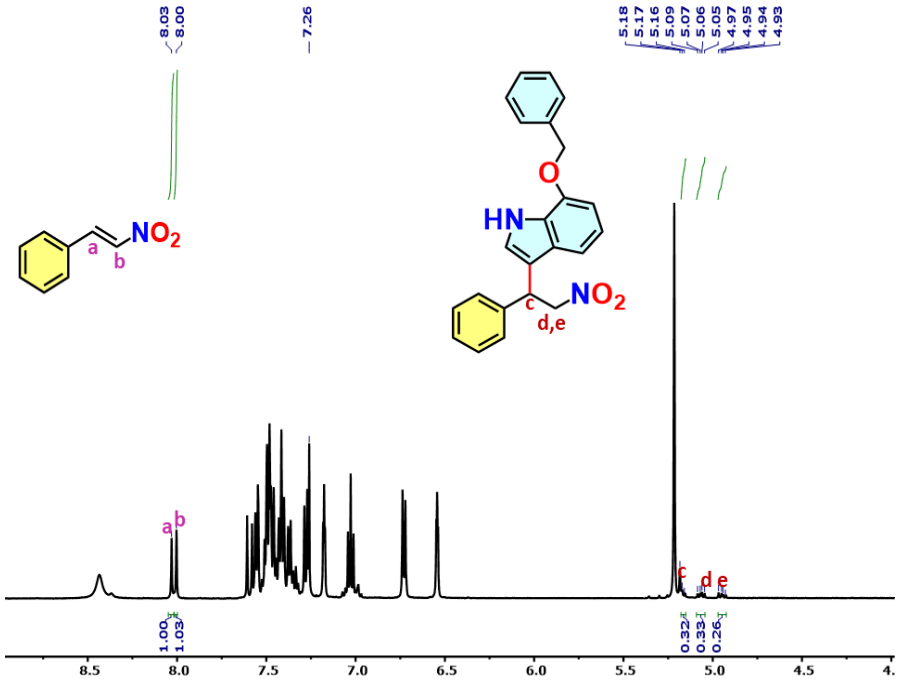

Fig. S18. Integration in the 1H NMR spectrum for the determination of conversion (%) of the reaction product catalyzed by **20a (Table 2, entry 5)**.

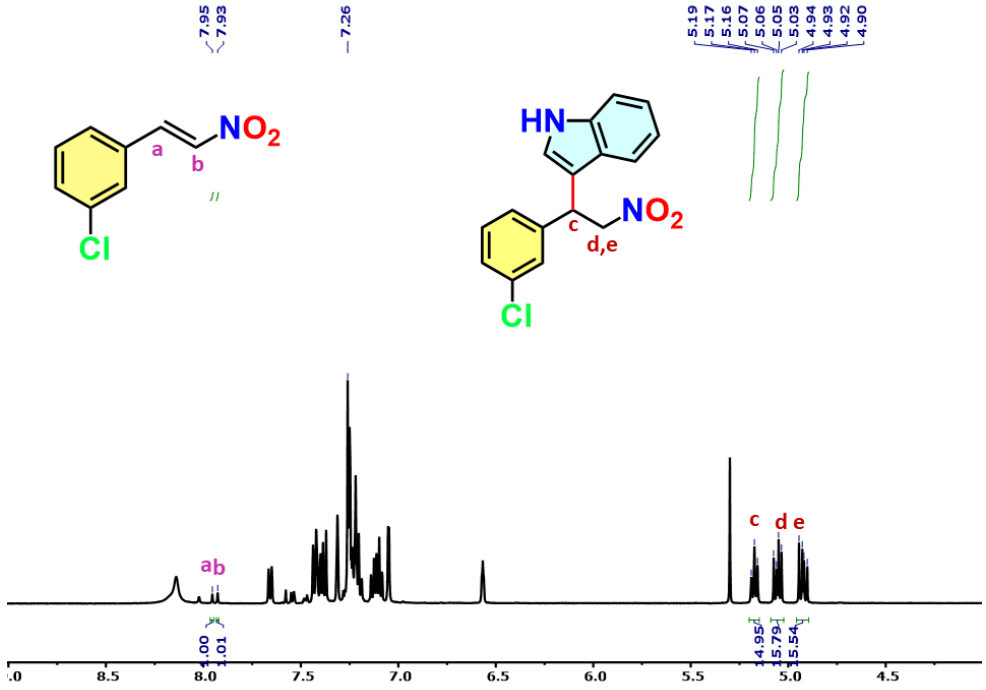

Fig. S19. Integration in the ^{1}H NMR spectrum for the determination of conversion (%) of the reaction product catalyzed by **20a** (**Table 3, entry 2**).

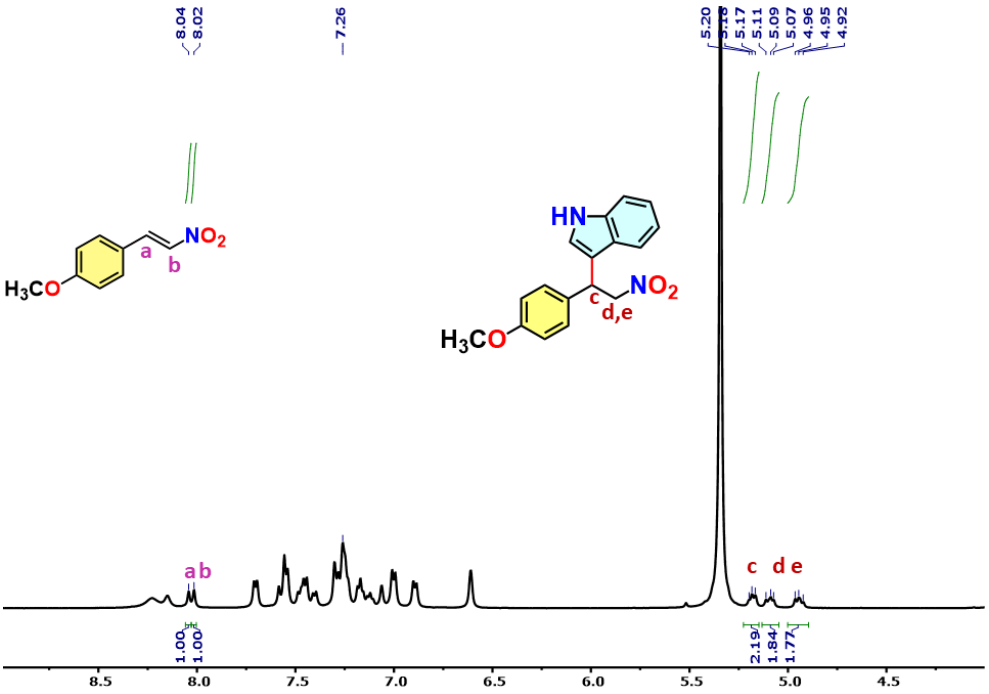

Fig. S20. Integration in the ^{1}H NMR spectrum for the determination of conversion (%) of the reaction product catalyzed by **20a** (**Table 3, entry 3**).

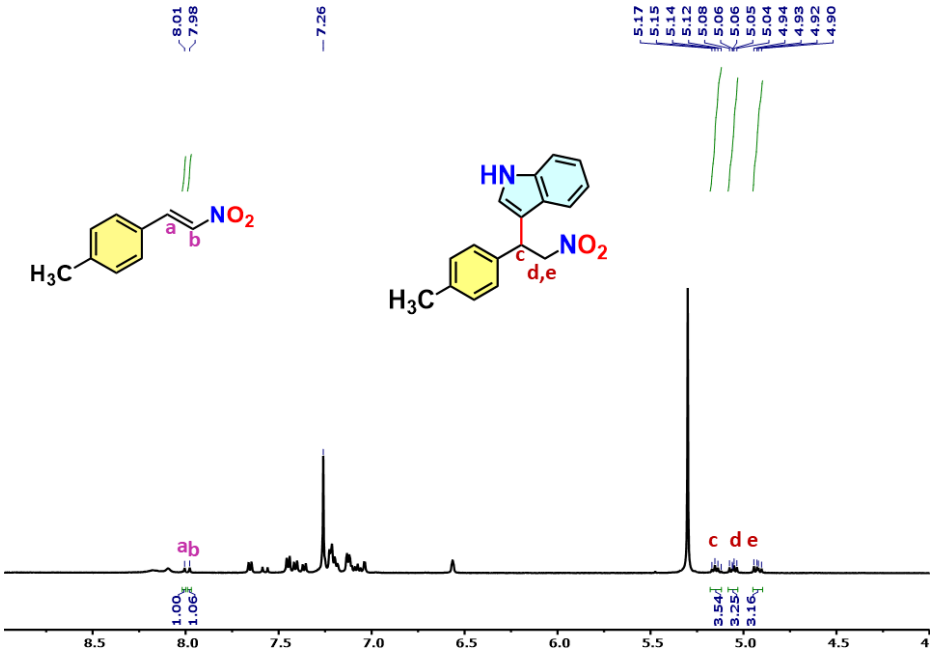

Fig. S21. Integration in the ^{1}H NMR spectrum for the determination of conversion (%) of the reaction product catalyzed by **20a** (**Table 3, entry 4**).

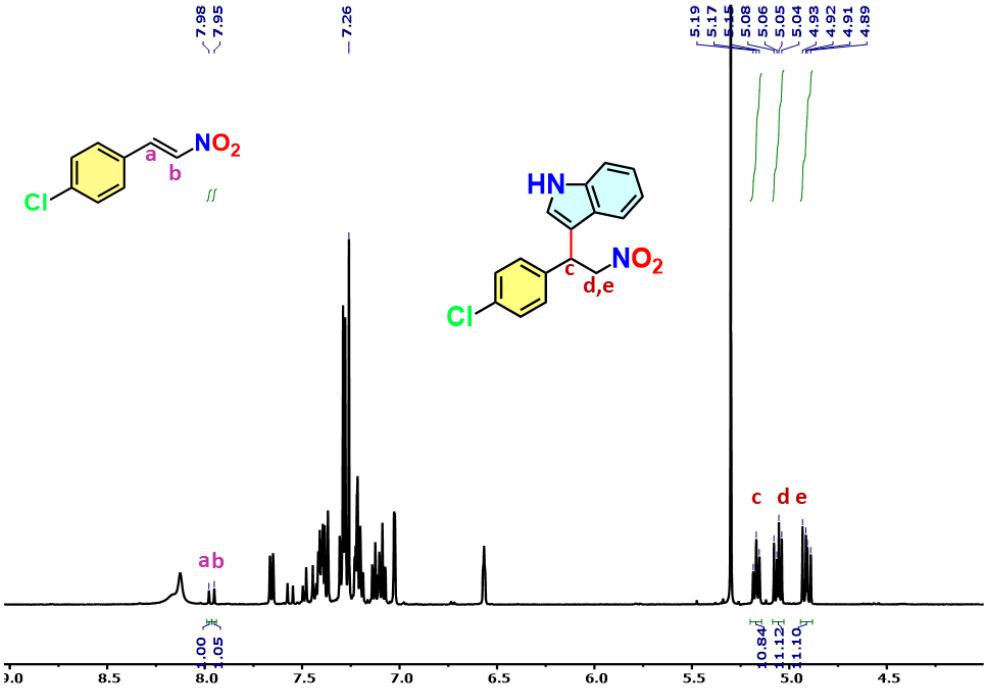

Fig. S22. Integration in the ^{1}H NMR spectrum for the determination of conversion (%) of the reaction product catalyzed by **20a** (**Table 3, entry 5**).

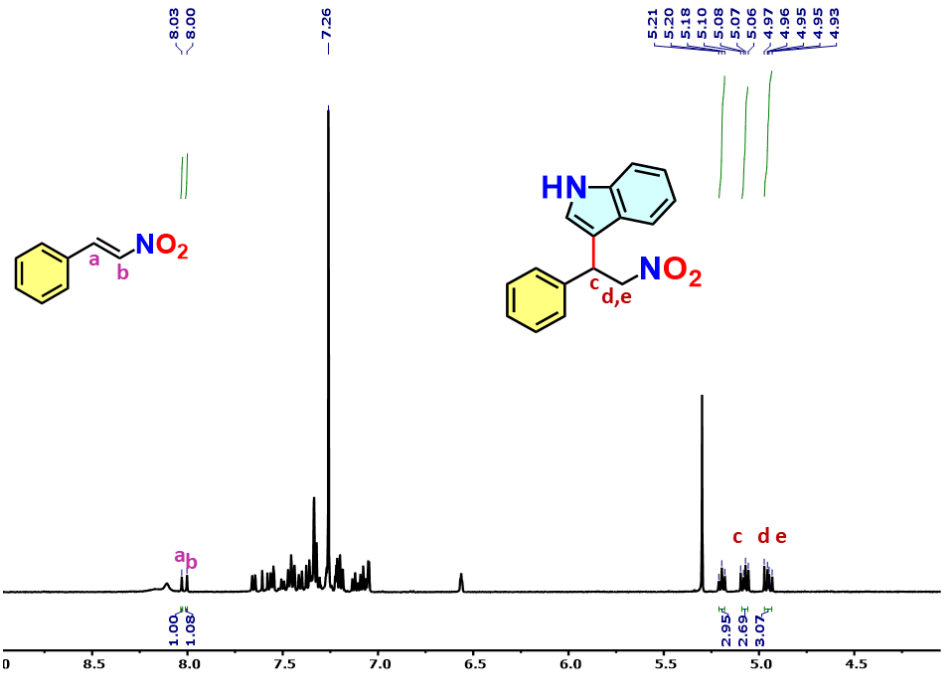

Fig. S23. Integration in the ^{1}H NMR spectrum for the determination of conversion (%) of the reaction product catalyzed by **20a** (**Table 1, entry NH_2BDC+BPY**).

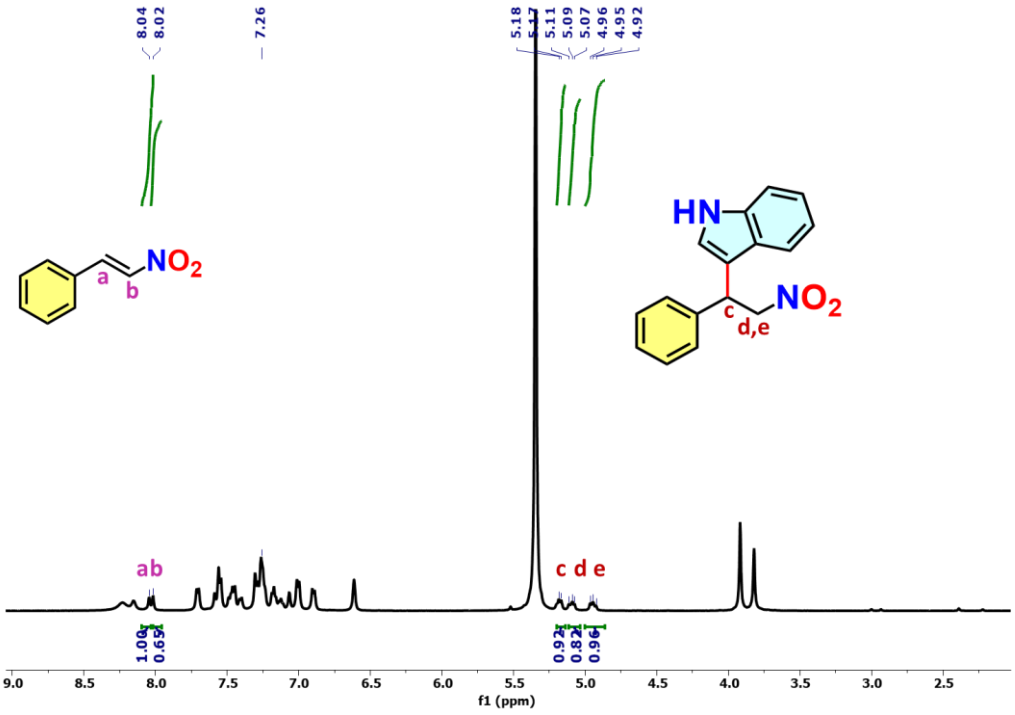

Fig. S24. Integration in the ^{1}H NMR spectrum for the determination of conversion (%) of the reaction product catalyzed by **20a** (**Table 1, entry BDC+NS**).

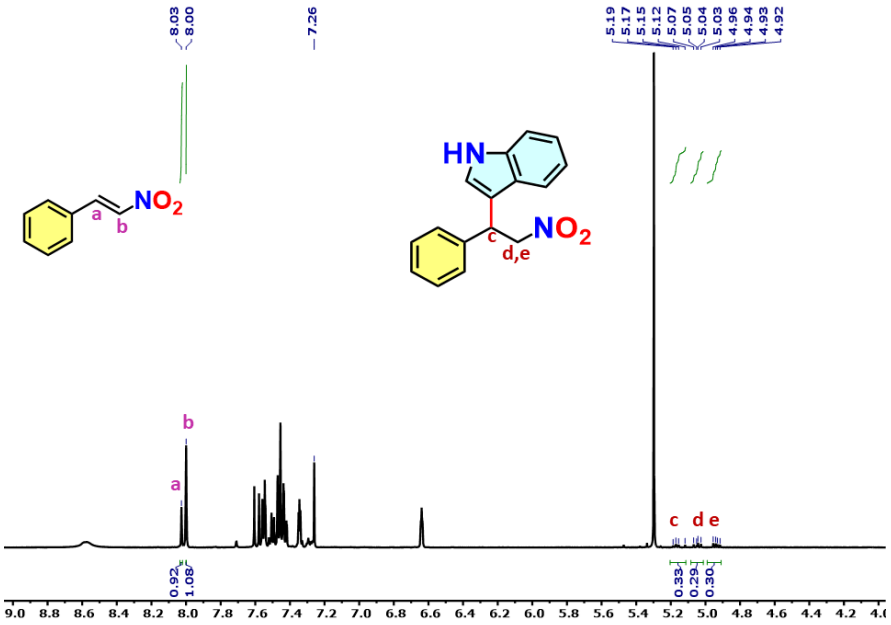

Fig. S25. Integration in the ^{1}H NMR spectrum for the determination of conversion (%) of the reaction product catalyzed by **20a** (**Table 1, entry BDC+BPY,**).

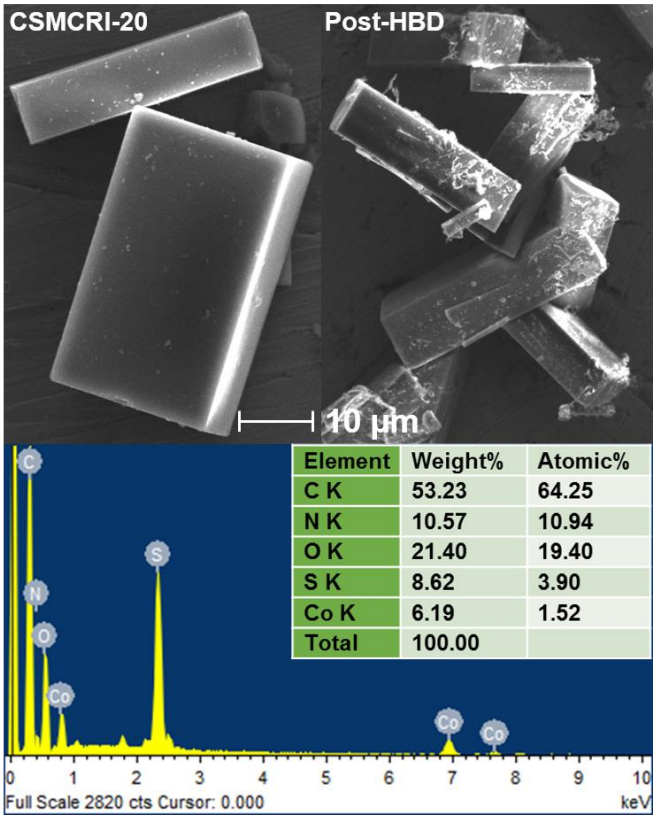

Element	Weight%	Atomic%
C K	53.23	64.25
N K	10.57	10.94
O K	21.40	19.40
S K	8.62	3.90
Co K	6.19	1.52
Total	100.00	

Fig. S26. FE-SEM images of **CSMCRI-20** (*top left*) and material after HBD catalysis (*top right*), revealing that block-shaped morphology is well retained. SEM-EDX analysis (below) of the material after HBD catalysis.

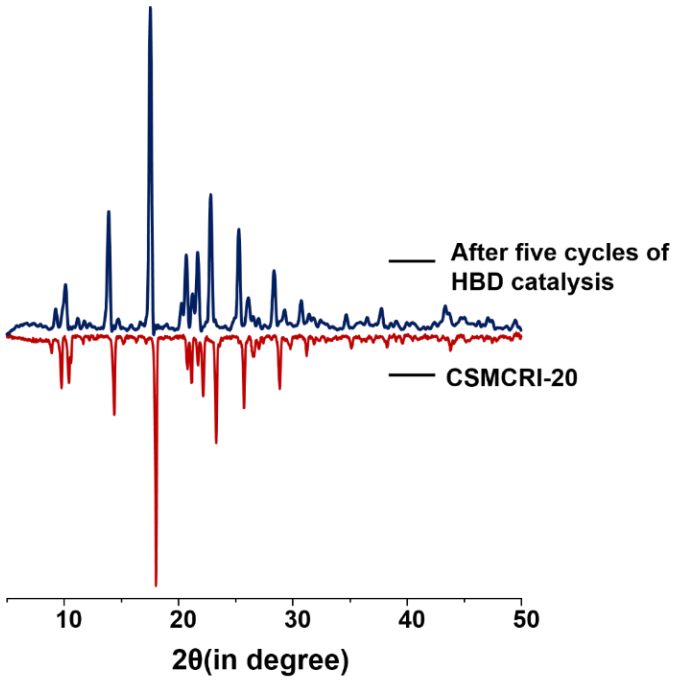

Fig. S27. PXRD pattern before and after HBD catalysis.

(a) (b)

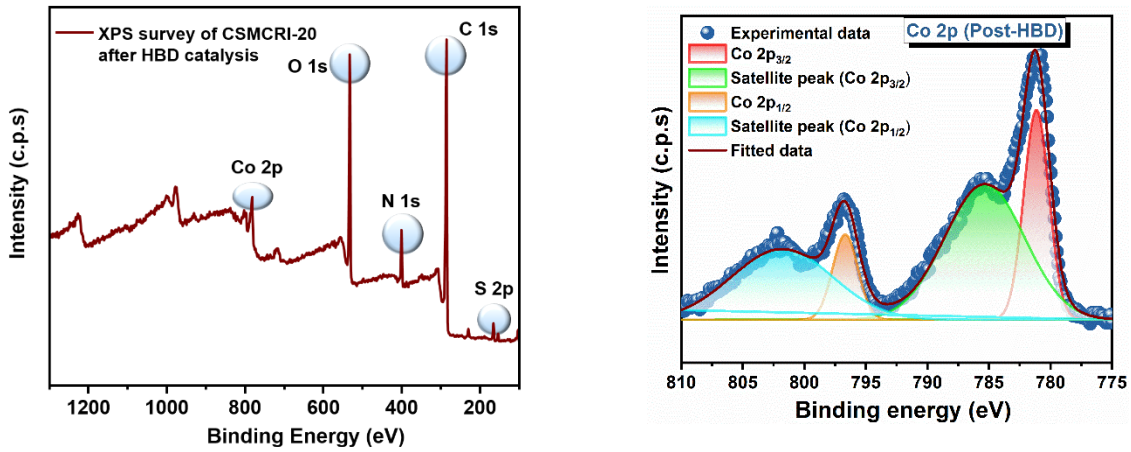

Fig. S28. a) XPS survey spectrum and b) High resolution deconvoluted Co 2p XPS spectrum after HBD analysis of **CSMCRI-20**.

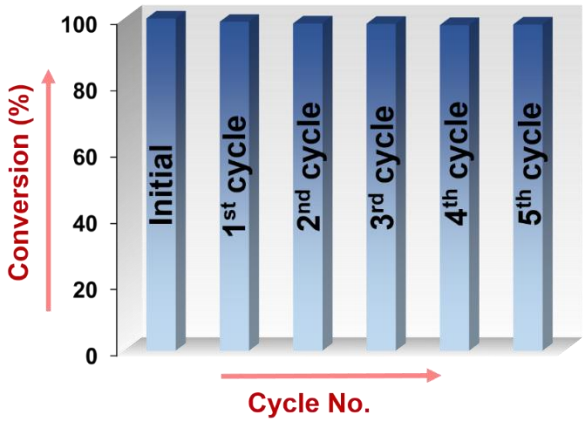

Fig. S29. Recyclability test along with conversion of the catalyst (**20a**) up to five cycles in HBD catalysis.

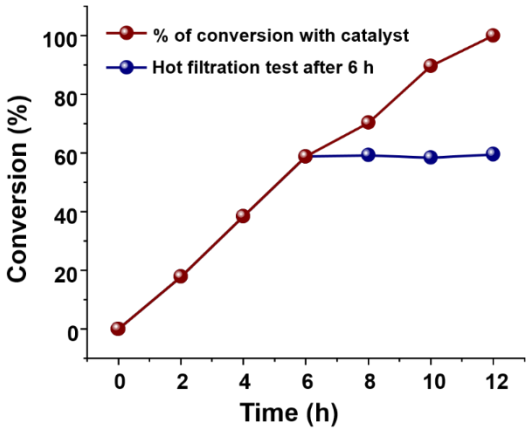

Fig. S30. Hot filtration test for HBD catalysis.

(a) (b)

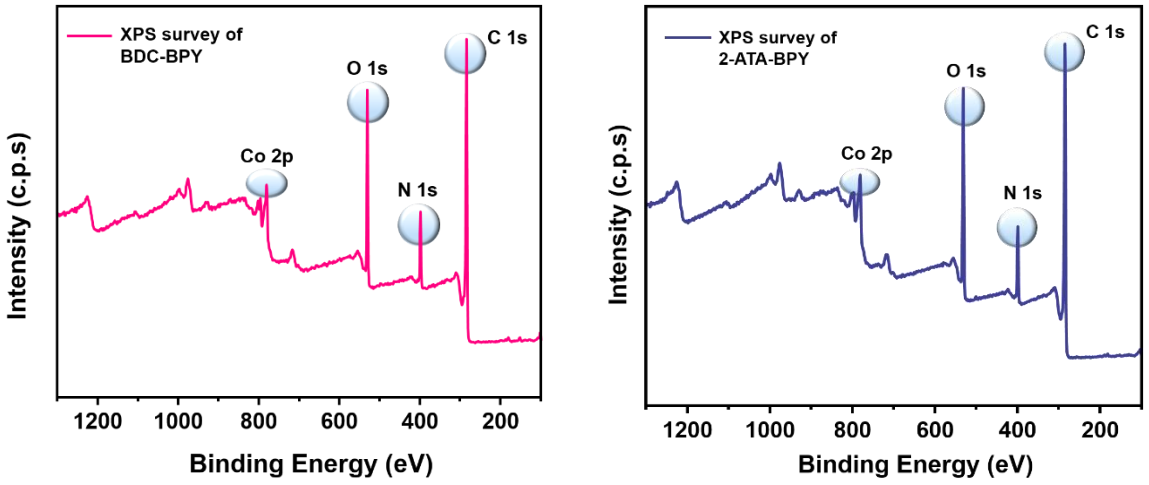

(c)

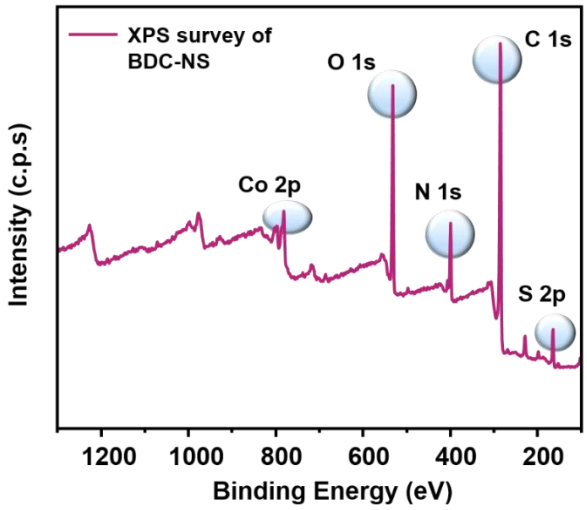

Fig. S31. a) XPS survey spectrum of three isostructural frameworks a) BDC-BPY, b) 2ATA-BPY and c) BDC-NS.

(a)

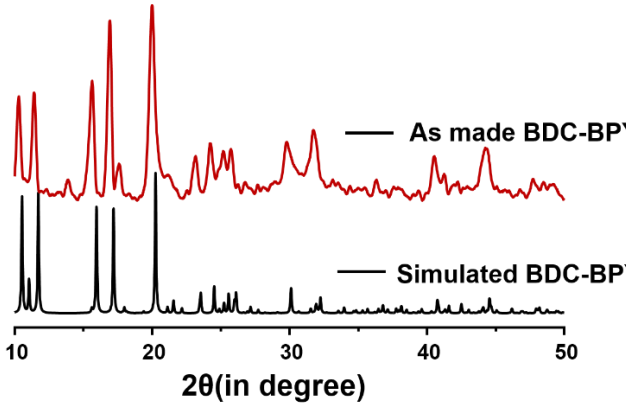

(b)

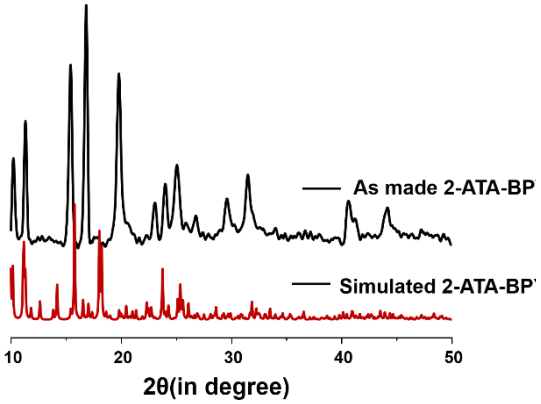

(c)

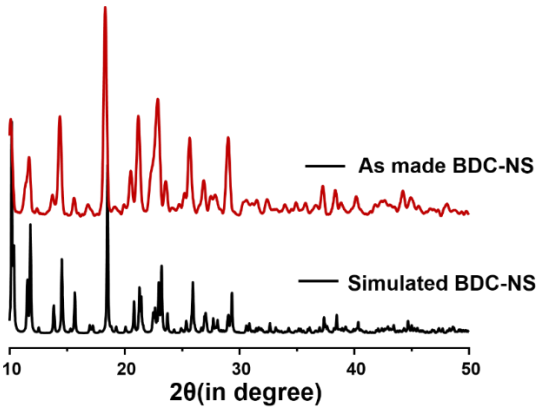

Fig. S32. a) Simulated and as made PXRD spectra of three isostructural frameworks a) BDC-BPY, b) 2ATA-BPY and c) BDC-NS.

Table S2. Crystal data and structure refinement for **CSMCRI-20**.

Identification code	**CSMCRI-20**
Empirical formula	$C_{22}H_{13}N_5O_4S_2Co$
Formula weight	534.42
Temperature/K	423.15
Crystal system	orthorhombic
Space group	*Pccn*
a/Å	17.201(2)
b/Å	18.3962(18)
c/Å	16.721(2)
α/°	90.00
β/°	90.00
γ/°	90.00
Volume/Å^3	5291.1(10)
Z	8
ρ_{calc}g/cm^3	1.342
μ/mm^{-1}	0.841
F(000)	2168.0
Crystal size/mm^3	0.9 × 0.173 × 0.036
Radiation	MoKα (λ = 0.71073)
2Θ range for data collection/°	4.06 to 56.66
Index ranges	-22 ≤ h ≤ 22, -22 ≤ k ≤ 24, -22 ≤ l ≤ 22
Reflections collected	115413
Independent reflections	6543 [R_{int} = 0.2937, R_{sigma} = 0.1143]
Data/restraints/parameters	6543/0/308
Goodness-of-fit on F^2	1.013
Final R indexes [I>=2σ (I)]	R_1 = 0.1113, wR_2 = 0.2922
Final R indexes [all data]	R_1 = 0.2180, wR_2 = 0.3814
Largest diff. peak/hole / e Å^{-3}	4.21/-0.87

Alert level A
RINTA01_ALERT_3_A The value of Rint is greater than 0.25
Rint given 0.294
PLAT020_ALERT_3_A The Value of Rint is Greater Than 0.12 ..... 0.294 Report
Alert level B
PLAT084_ALERT_3_B High wR2 Value (i.e. > 0.25) ..... 0.38 Report
PLAT094_ALERT_2_B Ratio of Maximum / Minimum Residual Density .... 4.86 Report
PLAT097_ALERT_2_B Large Reported Max. (Positive) Residual Density 4.21 eA^{-3}
PLAT220_ALERT_2_B NonSolvent Resd 1 N Ueq(max)/Ueq(min) Range 7.8 Ratio

PLAT234_ALERT_4_B Large Hirshfeld Difference N9 --C3 . 0.26 Ang
PLAT973_ALERT_2_B Check Calcd Positive Resid. Density on Co1 1.87 eA^{-3}

Explanation: These Alerts are generated due to disorder in the structure.

5. Determination of formula & solvent composition of CSMCRI-20 from PLATON squeeze and thermogravimetric analysis data:

From the TGA plot of as-synthesized **CSMCRI-20**, the observed mass loss is 11.52 %.Also, in the Co_2-SBU, So, formula of the asymmetric unit excluding the guest solvents is [Co(2ATA)(NS)].

From PLATON Squeeze program, void electron count excluding the guest molecules, comes out to be 270.

As **CSMCRI-20** is crystallized in orthorhombic space group *P*ccn (Z=8); so, number of void electron count per unit cell will be 270/8 = 33.75

Now, according to the above formula, mass of the asymmetric unit is 534.43 (**Table S2**).

Table S3. Number of electrons and molecular masses of guest solvent molecules associated with **CSMCRI-20** for determination of solvent composition and molecular formula.

	Dimethyl formamide (DMF)	Water
No. of electrons	40	10
Mass	73	18

Considering the above mentioned number of electrons, the best possible combination of solvent molecules for **CSMCRI-20** could be: [Co(2ATA)(NS)]·0.5DMF·1.5H_2O.

The total number of electrons contributed by lattice solvent molecules will be [(40×0.5) + (10×1.5)] = 35, which is in good agreement with the PLATON squeeze result and thus validates the above formula.

The aforementioned combination was further cross-checked from TGA analysis.

Mass loss due to guest solvents is [(73×0.5) + (18×1.5)] = 63.5

Therefore total mass of **CSMCRI-20** including the guests is (534.43+63.5) = 597.93

So mass loss due to guest and coordinated solvents is [(63.5/597.93)×100] % = 10.62 % which is in good agreement with that of the TGA result.

Table S4. A comparison of electrocatalytic performance of activated **CSMCRI-20** in water oxidation to that of other systems.

Sl. No.	Material	Overpotential (mV)@10 mA/cm^2	Tafel Slope (mV/dec)	TOF value (s^{-1})	Reference
1.	$Co_3(HITP)_2$	254 mV (pH 14.0)	86.5	-	*Appl. Catal., B*, **2020**, *278*, 119295.
2.	Co_2-MOF@Nafion	460@2 mA/cm^2 and 537@5 mA/cm^2 (pH 7.0)	105±5	0.026	*ACS Appl. Mater. Interfaces* **2019**, *11*, 46658−46665
3.	MOF-2	370@1 mA/cm^2 (pH 13.0)	101.9	0.6	*ACS Appl. Mater. Interfaces* **2020**, *12*, 33679−33689
4.	NH_2TA-Ni-MOF	356@1 mA/cm^2 (pH 13.0)	105	1.26×10^{-2}	*Chem. Eur. J.* **2019**, *25*, 11141 – 11146
5.	Co:Fe_3	453 mV	63	0.088	*J. Am. Chem. Soc.* ***2017***, *139*, *5*, 1778–1781
6.	UTSA-16	408 (pH 14.0)	77	-	*ACS Appl. Mater. Interfaces* **2017**, *9*, 7193−7201
7.	Co-TpBpy	400@1 mA/cm^2 (pH 7.0, buffer)	59	0.23	*Chem. Mater.* **2016**, *28*, 4375-4379
8.	Co-WOC-1	390@1 mA/cm^2 (pH 13.0)	128	0.05	*Angew. Chem., Int. Ed.* **2016**, *55*, 2425-2430
9.	Fe/Ni MOF Film	270 (pH 13.0)	47	0.13	*ACS Appl. Mater. Interfaces* **2016**, *8*, 16736−16743
10.	CSMCRI-10	396 (pH 14.0)	102	0.03	*Chemical Engineering Journal* **2022,** *429*, 132301.
11.	NG-$CoSe_2$	366	40	0.03	*ACS Nano* **2014**, *8*, 3970-3978
12.	**CSMCRI-20**	391 (pH 14.0)	85	4.03×10^{-4}	**This work**

Table S5. Comparison of Various HBD Catalysts in the Friedel−Crafts Alkylation Reaction of Indole and *β*-Nitro styrene

Entry	catalyst	mol (%)	time (h)	solvent	temp (°C)	yield (%)	ref.
1.	Zr-UiO-67-Urea	3.8	24	Toluene	70	97	*Inorganic Chemistry* **2019** ,*58*,5163-5172
2.	Cr-MIL-101-UR3	15	24	CH_3CN	60	93	*Chem. Commun.* **2013**,*49*, 7681−768
3.	{[Zn_2(BQBG)(BDC)$_2$].10H_2O}n	3	12	CH_2Cl_2	35	100	*ACS Catal.* **2019**, *9*,3165–3173
4.	Uio-67-Squar/bpdc	10	24	Toluene -d_8	50	95	J. Am. Chem.Soc. **2015**, *137*, 919–925
5.	Cu_4(dbda)$_2$·(CH_3OH)$_4$	5	24	$CHCl_3$	50	>99	*Chem. Commun.* **2016**, *52*, 8585−8588
6.	NU-GRH-1 + TMS-Cl	3	4	Toluene -d_8	60	98	*ACS Catal.* **2016**, *6*, 3248−3252
7.	[CuL_2·H_2O]·2DMF·H_2O	1.5	18	CH_3CN	60	98	*Catal. Commun.* **2018**, *104*, 123−127

8.	NU-601	10	36	$MeNO_2$/ THF	60	98	J. Am. Chem. Soc. **2012**, *134*,3334−3337
9.	**CSMCRI-20**	9	12	DCM	60	100	**Present work**

References

1. G. Sheldrick, SHELXS, University of Göttingen, Germany (1997);(c) W. Madison, Bruker APEX2 Software, Bruker AXS Inc. V2. 0-1, USA (2005);(d) GM Sheldrick, *J SADABS, Program for Empirical Absorption Correction of Area Detector Data*, 1997.
2. G. Sheldrick, SAINT and XPREP, version 5.1, *J Siemens Industrial Automation Inc., Madison, WI*, 1995.
3. S. Bruker, Bruker AXS Inc., Madison, Wisconsin, USA, Version 6.02 (includes XPREP and SADABS), 1999.
4. O. V. Dolomanov, L. J. Bourhis, R. J. Gildea, J. A. K. Howard and H. Puschmann, OLEX2: A Complete Structure Solution, Refinement and Analysis Program, *J. Appl. Crystallogr.*, 2009, **42**, 339.
5. G. Sheldrick, SHELXL-2014/7, University of Gottingen, Germany, 2014 Search PubMed;(b) L. Farrugia, *J. Appl. Crystallogr*, 2012, **45**, 849-854.
6. G. M. Sheldrick, Crystal Structure Refinement with SHELXL. Acta Crystallographica, *Acta Crystallogr., Sect. C: Struct. Chem.*, 2015, **71**, 3.
7. G. M. Sheldrick, Crystal Structure Refinement with SHELXL, *Acta Crystallogr., Sect. C: Struct. Chem.*, 2015, **71**, 3.
8. A. Spek, Single-Crystal Structure Validation with the Program Platon, *J. Appl. Crystallogr.*, 2003, **36**, 7-13.
9. V. A. Blatov, A. P. Shevchenko and D. M. Proserpio, Applied Topological Analysis of Crystal Structures with the Program Package TOPOSPRO, *Cryst. Growth Des.*, 2014, **14**, 3576-3586.
10. S. Millan, G. Makhloufi and C. Janiak, Incorporating the Thiazolo[5,4-d]thiazole Unit into a Coordination Polymer with Interdigitated Structure, *Crystals*, 2018, **8**, 30.